J|A|C|S ARTICLES

Published on Web 08/25/2010

Synthesis and Characterization of ERI-Type UZM-12 Zeolites and Their Methanol-to-Olefin Performance

Joo Hyuck Lee,[†] Min Bum Park,[†] Jun Kyu Lee,[†] Hyung-Ki Min,[†] Mee Kyung Song,[‡] and Suk Bong Hong*,[†]

Department of Chemical Engineering and School of Environmental Science and Engineering, POSTECH, Pohang 790-784, Korea, and Center for Nanomaterials, Sogang University, Seoul 121-742, Korea

Received June 14, 2010; E-mail: sbhong@postech.ac.kr

Abstract: A wide variety of different linear, diquaternary alkylammonium ions have been used as supplementary crystallization structure-directing agents (SDAs) in the synthesis of UZM-12, a high-silica version of zeolite erionite, via a charge density mismatch (CDM) approach. When tetraethylammonium is used as a CDM SDA, the crystallization of UZM-12 was found to be critically dependent not only on the type of alkali metal cations added as another crystallization SDA to the synthesis mixture, but also on the size of the groups on the diquaternary ammonium ion employed and the length of its central polymethylene chain that are closely related to the dimensions of cylindrical 23-hedral [$4^{12}6^58^6$] *eri* cages in this small-pore zeolite. ^{27}Al MQ MAS NMR measurements reveal a preferential location of Al on the high-multiplicity site over the lower-multiplicity site of the UZM-12 framework. The catalytic results from the methanol-to-olefin reaction over a series of H-UZM-12 zeolites with similar acidic properties but different crystallite sizes (100−2500 nm in length) demonstrate that the nanocrystallinity (probably the ≤100 nm range) may have a detrimental effect on the activity and stability for this reaction, probably due to the fast buildup of large coke molecules on the external surface of zeolite crystallites that inhibits the methanol diffusion to intrazeolitic acid sites, rendering them ultimately inaccessible for catalysis.

Introduction

UZM-12, which is a high-silica analogue of the rare natural zeolite erionite (framework type ERI), is among the aluminosilicate zeolites with already known framework structures but previously unobserved chemical compositions that workers at UOP have recently synthesized using the so-called charge density mismatch (CDM) approach.[1−3] This new strategy holds some degree of rational design for new zeolite structures, because it includes the objective of leading to a cooperative structure direction with multiple structure-directing agents (SDAs) and/or a more favorable match with the negative framework charge density of the resulting aluminosilicate product. The ERI structure consists of columns of 11-hedral [4^66^5] *can* cages that are joined by double 6-rings in the *c*-axis, while being alternatively rotated by 60°.[4] Adjacent columns are linked by single 6-rings connecting *can* cages at the same level, forming the larger cylindrical 23-hedral [$4^{12}6^58^6$] *eri* cages with 6.3 Å in diameter and 13.0 Å in height[5] that can be accessible through elliptical 8-ring (3.6 × 5.1 Å) windows. UZM-12 has been reported to crystallize at Si/Al ratios >5.5 through the combined use of tetraethylammonium (TEA^+) as a CDM SDA and *N*,*N*,*N*,*N*′,*N*′,*N*′-hexamethylbutanediammonium ($(CH_3)_3N^+(CH_2)_4N^+(CH_3)_3$, Me_6-diquat-4), *N*,*N*,*N*,*N*′,*N*′,*N*′-hexamethylhexanediammonium ($(CH_3)_3N^+(CH_2)_6N^+(CH_3)_3$, Me_6-diquat-6), or benzyltrimethylammonium ion as an organic crystallization SDA in the presence of K^+.[2] Also, this small-pore zeolite is known to vary in crystallite size and morphology from the micrometric to the nanometric range and from the spherical to needlelike shape, respectively, depending on the type of the organic crystallization SDA employed, as well as on the K^+/Al ratio of synthesis mixtures.

It is well-established that the use of organic SDAs with a high degree of flexibility and hydrophilicity, instead of conformationally rigid and bulky (and thus relatively hydrophobic) ones, in zeolite syntheses is another viable strategy for the discovery of previously unobserved framework structures.[6] In this respect, Me_6-diquat-6 is remarkable, because it can direct the formation of a number of different zeolite structures: EU-1 (EUO), ZSM-12 (MTW), ZSM-23 (MTT), NU-87 (NES), and ZSM-48 (*MRE) in alkaline media[7] and various new phases

[†] POSTECH.
[‡] Sogang University.

(1) (a) Blackwell, C. S.; et al. *Angew. Chem., Int. Ed.* **2003**, *42*, 1737. (b) Lewis, G. J.; Miller, M. A.; Moscoso, J. G.; Knight, L. M.; Wilson, S. T. *Stud. Surf. Sci. Catal.* **2004**, *154*, 364. (c) Miller, M. A.; Moscoso, J. G.; Koster, S.; Gatter, M. G.; Lewis, G. J. *Stud. Surf. Sci. Catal.* **2007**, *170*, 347.
(2) (a) Miller, M. A.; Lewis, G. J.; Moscoso, J. G.; Koster, S.; Modica, F.; Gatter, M. G.; Nemeth, L. T. *Stud. Surf. Sci. Catal.* **2007**, *170*, 487. (b) Miller, M. A.; Lewis, G. J.; Gisselquist, J. L.; Moscoso, J. G.; Patton, R. L. U.S. Patent 7,344,694, 2008.
(3) Kim, S H.; Park, M. B.; Min, H.-K.; Hong, S. B. *Microporous Mesoporous Mater.* **2009**, *123*, 160.
(4) Baerlocher, Ch.; McCusker, L. B. Database of Zeolite Structures; http://www.iza-structure.org/databases/.
(5) Proefschrift, A. Ph.D. Thesis; University of Amsterdam, 2005.
(6) Hong, S. B. *Catal. Surv. Asia* **2008**, *12*, 131.
(7) (a) Casci, J. L.; Lowe, B. M.; Whitttam, T. V. U.S. Patent 4,537,754, 1985. (b) Moini, A.; Schmitt, K. D.; Valyocsik, E. W.; Polomski, R. F. *Zeolites* **1994**, *14*, 504.

including ITQ-13 or IM-7 (ITH), ITQ-22 (IWW), ITQ-24 (IWR), IM-10 (UOZ), and ITQ-33 when combined with the structure-directing effects of F^- and/or Ge.[8] Among those organic SDAs studied thus far, however, of the greatest success story may be the $(C_5H_{11})N^+(CH_2)_nN^+(C_5H_{11})$ ions with $n = 4-6$, composed of two 1-methylpyrrolidinium groups connected by tetra-, penta-, and hexamethylene chains, which yield novel medium-pore materials TNU-9 (TUN), IM-5 (IMF), and SSZ-74 (-SVR), respectively.[9−11] In fact, a series of our studies on zeolite syntheses using such flexible, linear diquaternary alkylammonium ions as organic SDAs has shown that the phase selectivity of the crystallization can be altered according not only to the oxide composition of synthesis mixtures, but also to the length of the central polymethylene chain of the diquaternary ammonium ion employed and the size of its aliphatic or cyclic moieties.[6,9,12−15]

The purpose of the present study is to investigate the effects of both inorganic and organic synthetic parameters on the crystallization of UZM-12 using a CDM approach. Here we have tested the ability of a large number of diquaternary alkylammonium ions with different central chain lengths and end group sizes as organic crystallization SDAs in UZM-12 synthesis, with TEA^+ and K^+ ions present as a CDM SDA and an inorganic crystallization SDA, respectively. We have also attempted to crystallize this small-pore zeolite in the presence of various alkali metal cations other than K^+ in combination with TEA^+ and one of diquaternary ammonium ions prepared here. The UZM-12 zeolites crystallized are characterized by using powder X-ray diffraction, computer modeling studies, elemental and thermal analyses, scanning electron microscopy, multinuclear MAS NMR, ^{27}Al MQ MAS NMR, N_2 sorption, and temperature-programmed desorption of ammonia. In particular, the materials with similar Si/Al ratios but different crystallite sizes (0.1−2.5 μm in length) are tested as catalysts for the methanol-to-olefin (MTO) reaction that has been steadily regarded as an alternative technology to produce ethene and propene from nonpetroleum sources such as natural gas and coal.[16] Their catalytic results are compared to those obtained from H-SAPO-34 (CHA), H-SAPO-17 (ERI), and H-SSZ-13 (CHA) which are the best and the most widely studied catalysts for this reaction, the silicoaluminophosphate counterpart of H-UZM-12, and the aluminosilicate one of H-SAPO-34, respectively.[4,16] We also use gas chromatography−mass spectroscopy (GC−MS) to identify the hydrocarbon species formed on these zeolitic materials during MTO.

Experimental Section

Organic SDA Synthesis. Six series of diquaternary alkylammonium ions characterized by different types of the end groups containing the charged nitrogen, i.e., *N*,*N*,*N*,*N*′,*N*′,*N*′-hexamethylalkanediammonium ($(CH_3)_3N^+(CH_2)_nN^+CH_3)_3$, Me_6-diquat-*n* with $n = 3-8$), *N*,*N*,*N*′,*N*′-tetramethyl-*N*,*N*′-diethylalkanediammonium ($(CH_3)_2(C_2H_5)N^+(CH_2)_nN^+(C_2H_5)(CH_3)_2$, Me_4Et_2-diquat-*n* with $n = 3-8$), *N*,*N*,*N*′,*N*′-tetraethyl-*N*,*N*′-dimethylalkanediammonium ($(C_2H_5)_2(CH_3)N^+(CH_2)_nN^+(CH_3)(C_2H_5)_2$, Et_4Me_2-diquat-*n* with $n = 3-6$), *N*,*N*,*N*,*N*′,*N*′,*N*′-hexaethylalkanediammonium $(C_2H_5)_3N^+(CH_2)_nN^+(C_2H_5)_3$, Et_6-diquat-*n* with $n = 3-6$), 1,*n*-bis(*N*-methylpyrrolidinium)alkane ($(C_5H_{11})N^+(CH_2)_nN^+(C_5H_{11})$, MPr_2-diquat-*n* with $n = 3-8$), and 1,*n*-bis(*N*-methylpiperidinium)alkane ($(C_6H_{13})N^+(CH_2)_nN^+(C_6H_{13})$, MPp_2-diquat-*n* with $n = 3-8$) ions were prepared and recrystallized according to the procedures described in our previous studies.[9,12−15] After purification, the formation and purity of the dibromide salt of 32 different organic species described above were confirmed by ^{1}H and ^{13}C NMR and stored in a desiccator prior to their use as crystallization SDAs.

Zeolite Synthesis. The reagents used for UZM-12 synthesis included diquaternary cations prepared here, tetraethylammonium hydroxide (TEAOH, 35% aqueous solution, Aldrich), aluminum tri*sec*-butoxide ($Al[OCH(CH_3)C_2H_5]_3$, 97%, Aldrich), colloidal silica (Ludox AS-40, DuPont) and the chlorides of Li^+, Na^+, K^+, Rb^+ and Cs^+ ions. The final composition of the synthesis mixture was $13.0TEAOH \cdot 2.0RBr_2 \cdot 1.5MCl \cdot 0.5Al_2O_3 \cdot 16SiO_2 \cdot 400H_2O$, where R is diquaternary alkylammonium ion and M is Li^+, Na^+, K^+, Rb^+ or Cs^+, respectively. After being stirred at room temperature for 1 day, the synthesis mixture was charged into Teflon-lined 45-mL autoclaves and heated at 100 °C, with rotating (60 rpm), for 7−35 days. For comparison, some syntheses were carried out after the diquaternary cation in synthesis mixtures was replaced by their specific precursors: for example, 1,6-dibromohexane (1,6-DBH, 96%, Aldrich) and trimethylamine (TMA, 33% solution in ethanol, Aldrich) instead of Me_6-diquat-6. In this set of synthesis experiments, the gel composition was fixed to $13.0TEAOH \cdot 2.0P_1 \cdot 6.0P_2 \cdot 1.5KCl \cdot 0.5Al_2O_3 \cdot 16SiO_2 \cdot 400H_2O$, where P_1 and P_2 are α,ω-dibromoalkane and aliphatic or cyclic triamine, respectively. The solid products were recovered by filtration or centrifugation, washed repeatedly with water, and then dried overnight at room temperature.

As-made UZM-12 was calcined in air at 550 °C for 8 h and refluxed twice in 1.0 M NH_4NO_3 solutions (1.0 g solid per 100 mL solution) for 6 h followed by calcinations at 550 °C for 4 h in order to obtain its proton form (i.e., H-UZM-12). For catalytic comparison, two SAPO-34 materials with similar Si contents but different crystallite sizes (1 and 2−4 μm, respectively) were synthesized via a double organic SDA strategy.[17] Here we refer to the materials with small and large crystallite sizes as SAPO-34(I) and SAPO-34(II), respectively. In addition, SAPO-17 and SSZ-13 were prepared and converted into their proton form following the procedures previously reported.[18,19]

(8) (a) Corma, A. In *Proceedings of the 14th International Zeolite Conference*; van Steen, E., Callanan, L. H., Claeys, M., Eds.; Document Transformation Technologies: Cape Town, 2004; p 25. (b) Mathieu, Y.; Pailaud, J. L.; Caullet, P.; Bats, N. *Microporous Mesoporous Mater.* **2004**, *75*, 13. (c) Corma, A.; Diaz-Cabanas, M.; Jorda, J.; Martinez, C.; Moliner, M. *Nature* **2006**, *443*, 842.
(9) (a) Hong, S. B.; Lear, E. G.; Wright, P. A.; Zhou, W.; Cox, P. A.; Shin, C.-H.; Park, J.-H.; Nam, I.-S. *J. Am. Chem. Soc.* **2004**, *126*, 5817. (b) Gramm, F.; Baerlocher, Ch.; McCusker, L. B.; Warrender, S. J.; Wright, P. A.; Han, B.; Hong, S. B.; Liu, Z.; Ohsuna, T.; Terasaki, O. *Nature* **2006**, *44*, 79. (c) Hong, S. B.; Min, H.-K.; Shin, C.-H.; Cox, P. A.; Warrender, S. J.; Wright, P. A. *J. Am. Chem. Soc.* **2007**, *129*, 10870.
(10) Baerlocher, Ch.; Gramm, F.; Massüger, L.; McCusker, L. B.; He, Z.; Hovmöller, S.; Zou, X *Science* **2007**, *315*, 1113.
(11) Baerlocher, Ch.; Xie, D.; McCusker, L. B.; Hwang, S.-J.; Wong, K.; Burton, A. W.; Zones, S. I. *Nat. Mater.* **2008**, *7*, 631.
(12) (a) Lee, S.-H.; Shin, C.-H.; Hong, S. B. *Chem. Lett.* **2003**, *32*, 542. (b) Lee, S.-H.; Shin, C.-H.; Yang, D.-K.; Ahn, S.-D.; Nam, I.-S.; Hong, S. B. *Microporous Mesoporous Mater.* **2004**, *68*, 97. (c) Shin, J.; Hong, S. B. *Microporous Mesoporous Mater.* **2009**, *124*, 227.
(13) (a) Paik, W. C.; Shin, C.-H.; Hong, S. B. *Chem. Commun.* **2000**, 1609. (b) Lee, S.-H.; Lee, D.-K.; Shin, C.-H.; Paik, W. C.; Lee, W. M.; Hong, S. B. *J. Catal.* **2000**, *196*, 158. (c) Lee, S.-H.; Shin, C.-H.; Choi, G. J.; Park, T.-J.; Nam, I.-S.; Han, B.; Hong, S. B. *Microporous Mesoporous Mater.* **2003**, *60*, 237.
(14) Lee, S.-H.; Lee, D.-K.; Shin, C.-H.; Park, Y. K.; Wright, P. A.; Lee, W. M.; Hong, S. B. *J. Catal.* **2003**, *215*, 151.
(15) (a) Han, B.; Lee, S.-H.; Shin, C.-H.; Cox, P. A.; Hong, S. B. *Chem. Mater.* **2005**, *17*, 477. (b) Han, B.; Shin, C.-H.; Nam, I.-S.; Hong, S. B. *Stud. Surf. Sci. Catal.* **2005**, *158*, 183.
(16) (a) Stöcker, M. *Microporous Mesoporous Mater.* **1999**, *29*, 3. (b) Haw, J. F.; Song, W.; Marcus, D. M.; Micholas, J. B. *Acc. Chem. Res.* **2003**, *36*, 317.
(17) (a) Lee, K. Y.; Chae, H.-J.; Jeong, S.-Y.; Seo, G. *Appl. Catal., A* **2009**, *369*, 60. (b) Mertens, M.; Stromaier, K. G. U.S. Patent 6,773,688, 2004.
(18) Prakash, A. M.; Kevan, L. *Langmuir* **1997**, *13*, 5341.

Analytical Methods. Powder X-ray diffraction (XRD) patterns were measured on a PANalytical X'Pert diffractometer with an X'Celerator detector. Data were collected with a fixed divergence slit (0.50°) and Soller slits (incident and diffracted = 0.04 rad) and Cu K_α radiation. Elemental analysis for Si, Al, and alkali metal cations was performed on a Jarrell-Ash Polyscan 61E inductively coupled plasma spectrometer in combination with a Perkin-Elmer 5000 atomic absorption spectrophotometer. The C, H, and N contents of the samples were analyzed by using a Vario EL III elemental organic analyzer. Thermogravimetric analyses (TGA) were performed on an SII EXSTAR 6000 thermal analyzer, where the weight losses related to the combustions of organic SDAs or coke deposits formed during MTO were further confirmed by differential thermal analyses (DTA) using the same analyzer. Crystal morphology and average size were determined by a JEOL JSM-6510 scanning electron microscope (SEM). The N_2 sorption experiments were carried out on a Mirae SI nanoPorosity-XQ analyzer. Acidic properties of zeolitic materials prepared here were determined by temperature-programmed desorption (TPD) of pread-sorbed NH_3. The TPD was performed on a homemade experimental setup equipped with a thermal conductivity detector, following the procedure described in our recent work.[20]

The $^1H-^{13}C$ CP MAS and ^{13}C MAS NMR spectra at a spinning rate of 6.0 kHz were recorded on a Varian Inova 300 spectrometer at a ^{13}C frequency of 75.428 MHz with a $\pi/2$ rad pulse length of 7.0 μs. The $^1H-^{13}C$ CP MAS NMR spectra were obtained with an acquisition of ~5000 pulse transients, which was repeated with a contact time of 1 ms and a recycle delay of 3 s. For ^{13}C MAS NMR experiments, ca. 10000 pulse transients were accumulated with a recycle delay of 5 s. The ^{29}Si MAS NMR spectra at a spinning rate of 6.0 kHz were measured on the same spectrometer at a ^{29}Si frequency of 59.590 MHz. The spectra were obtained with an acquisition of 1000−2500 pulse transients, which was repeated with a $\pi/2$ rad pulse length of 7.0 μs and a recycle delay of 30 s. Spectral deconvolution and simulation were performed using the PeakFit curve-fitting program. The ^{13}C and ^{29}Si chemical shifts are reported relative to TMS. The ^{27}Al MAS NMR spectra at a spinning rate of 6.0 kHz were measured at a ^{27}Al frequency of 78.156 MHz with a $\pi/8$ rad pulse length of 1.8 μs and a recycle delay of 0.5 s, and an acquisition of ~5000 pulse transients. The ^{27}Al chemical shifts are reported relative to an $Al(H_2O)_6^{3+}$ solution. The ^{27}Al 3Q MAS NMR spectra were recorded on a Bruker AMX-400 FT-NMR spectrometer using a three-pulse *z*-filtered procedure at a spinning speed of 12.0 kHz.[21] The *z*-filter 3Q MAS sequence was employed to obtain a pure absorption mode 2D contour plot with negligible phase distortion, which was obtained by the equal jumps involved in the echo and antiecho coherence transfer pathways. The phase-sensitive 2D ^{27}Al 3Q MAS NMR measurements were conducted using the hyper-complex states procedure,[22] and their further details are described in our previous paper.[23] Quantification of the ^{27}Al resonances was done by a computer fitting of the corresponding 1D MAS NMR spectra using the quadrupolar parameters determined from the 3Q MAS NMR experiments.

To determine the energy-minimized conformations of different organic SDAs within the *eri* cages of UZM-12 zeolites, we carried out molecular modeling studies using the Buchart 1.02-Universal 1.01 force field as implemented in the Cerius^2 software.[24] The unit cell parameters and atomic coordinates for the ERI structure with space group $P6_3/mmc$ were taken from the original reference listed in the International Zeolite Association (IZA) tabulation.[4] The ERI unit cell structure was expanded to $1 \times 1 \times 2$ to build its pure-silica model ($Si_{72}O_{144}$). The host zeolite lattice was held fixed throughout the Monte Carlo (MC) simulation, while the organic SDA, occluded as one molecule per *eri* cage, was mobile to calculate the total interaction energy. The Lennard-Jones (L-J)-type potential energy function was used to describe the van der Waals (vdW) interactions, and the geometric combination rule was applied for the vdW interaction parameters. The cutoff distance for a short-range L-J summation in the MC simulation was 15 Å, and the total length of the run was 3×10^6. Every 5000th conformation was saved for the run, and hence, a total of 600 conformations were analyzed by energy. The final saved conformation was then minimized using the conjugated gradient algorithm. This minimized structure was further used for molecular dynamics simulations at 100 °C and a time step of 1 fs, using the Cerius^2 software on an SGI Origin300 8-CPU cluster in order to calculate the stabilization energies of organic SDAs within the *eri* cages of UZM-12. The system was equilibrated for 30 ps, and the ensemble-averaged values were obtained for a subsequent 100-ps run. Every 250th femtosecond configuration was saved during the run, and total of 400 configurations were saved as a trajectory file for the subsequent ensemble-averaged value analysis.

The coke materials formed on the zeolitic catalysts after MTO at 350 °C for different periods of time on stream (TOS) were extracted by a modification of the procedure originally developed by Guisnet group,[25] and their GC−MS total ion chromatograms were recorded on a Varian CP 3800 gas chromatograph equipped with a Varian 320-MSD mass selective detector, using electron impact ionization at 70 eV. The split ratio was 100:1, and the column used was a VF-5 capillary column (30 m × 0.25 mm) with flowing He (0.3 $cm^3\ min^{-1}$). The temperature program ramps the column from 70 to 280 °C at a rate of 4 °C min^{-1}. The organic compounds extracted were identified in comparison with the NIST database.[26]

Catalysis. A conventional continuous-flow microreactor was used to carry out MTO over various zeolitic catalysts at atmospheric pressure. Prior to the experiments, the catalyst was routinely activated under flowing N_2 (130 $cm^3\ min^{-1}$) at 550 °C for 2 h and kept at 350 °C to establish a standard operating procedure, allowing time for the reactant/carrier gas distribution to be stabilized. Then, methanol (MeOH) vapor was fed at a rate of 0.085 $cm^3\ h^{-1}$ (0.67 h^{-1} WHSV (weight hourly space velocity) into the reactor containing 0.1 g of catalyst at the same temperature. The total gas flow at the reactor inlet was kept constant at 30 $cm^3\ min^{-1}$. The reaction products were analyzed online in a Varian CP-3800 gas chromatograph equipped with a CP-PoraPLOT Q capillary column (0.25 mm ×25 m) and a flame ionization detector, with the first analysis carried out after 5 min on stream. CO_2 was separated using a packed Carbosphere column and analyzed with a thermal conductivity detector. Conversion was defined as the percentage of MeOH consumed during MTO. Dimethylether (DME) was not considered as a product. The yield of each product was calculated as the percentage of the amount (in mol) of MeOH converted to hydrocarbons.

Results and Discussion

Table 1 lists the results from syntheses using different diquaternary alkylammonium ions and alkali metal cations as organic and inorganic crystallization SDAs, respectively, under the conditions described above. In each case, the products listed were the only ones obtained in repeated trials. Our initial attempts to obtain UZM-12 were made to perform the crystallization using a potassium aluminosilicate synthesis mixture,

(19) Zones, S. I. U.S. Patent 4,544,538, 1985.
(20) Min, H.-K.; Park, M. B.; Hong, S. B. *J. Catal.* **2010**, *271*, 186.
(21) (a) Frydman, L.; Hardwood, J. S. *J. Am. Chem. Soc.* **1995**, *117*, 5367. (b) Amoureux, J. P.; Fernandez, C.; Steuernagel, S. *J. Magn. Reson.* **1996**, *123*, 116.
(22) States, D.; Haberkorn, R.; Ruben, D. *J. Magn. Reson.* **1982**, *48*, 286.
(23) Abraham, A.; Lee, S.-H.; Shin, C.-H.; Hong, S. B.; Prins, R.; van Bokhoven, J. A. *Phys. Chem. Chem. Phys.* **2004**, *6*, 3031.
(24) (a) de Vos Burchart, E.; Verheij, V. A.; van Bekkkum, H.; van de Graaf, B. *Zeolites* **1992**, *12*, 183. (b) Rappe, A. K.; Casewit, C. J.; Colwell, K. S.; Goddard, W. A.; Skiff, W. M. *J. Am. Chem. Soc.* **1992**, *114*, 10024. (c) *Cerius^2*, version 4.10; Accelrys: San Diego, CA.
(25) Guisnet, M.; Magnoux, P. *Appl. Catal.* **1989**, *54*, 1.
(26) NIST Chemistry WebBook; http://webbook.nist.gov/chemistry/.

Table 1. Representative Synthesis Results[a,b]

	alkali metal cations used as a crystallization SDA				
diquaternary cation used	K^+	Li^+	Na^+	Rb^+	Cs^+
Me_6-diquat-3	amorphous				
Me_6-diquat-4	UZM-12	D	amorphous[e]	UZM-12	analcime
Me_6-diquat-5	UZM-12				
Me_6-diquat-6	UZM-12	D	amorphous[e]	UZM-12	analcime
Me_6-diquat-7	UZM-12[c]				
Me_6-diquat-8	—[d]				
Me_4Et_2-diquat-3	amorphous				
Me_4Et_2-diquat-4	UZM-12	D	amorphous[e]	UZM-12	analcime
Me_4Et_2-diquat-5	UZM-12				
Me_4Et_2-diquat-6	UZM-12[c]				
Me_4Et_2-diquat-7	amorphous[e]				
Me_4Et_2-diquat-8	amorphous[e]				
Et_4Me_2-diquat-3	amorphous				
Et_4Me_2-diquat-4	UZM-12	L[c]	amorphous[e]	UZM-12	analcime
Et_4Me_2-diquat-5	UZM-12[e]				
Et_4Me_2-diquat-6	—[d]				
Et_6-diquat-3	amorphous[e]				
Et_6-diquat-4	amorphous[e]			amorphous[e]	
Et_6-diquat-5	—[d]				
Et_6-diquat-6	—[d]				
MPr_2-diquat-3	—[d]				
MPr_2-diquat-4	UZM-12	D	amorphous[e]	UZM-12	analcime
MPr_2-diquat-5	UZM-12				
MPr_2-diquat-6	UZM-12[e]				
MPr_2-diquat-7	amorphous[e]				
MPr_2-diquat-8	amorphous[e]				
MPp_2-diquat-3	amorphous				
MPp_2-diquat-4	UZM-12	L[c]	amorphous[e]	UZM-12	analcime
MPp_2-diquat-5	UZM-12[e]				
MPp_2-diquat-6	—[d]				

[a] The oxide composition of synthesis mixtures is $13TEAOH \cdot 2RBr_2 \cdot 1.5MCl \cdot 0.5Al_2O_3 \cdot 16SiO_2 \cdot 400H_2O$, where R is diquaternary alkylammonium ion and M is Li^+, Na^+, K^+, Rb^+, or Cs^+. Crystallization was performed under rotation (60 rpm) at 100 °C for 14 days, unless otherwise stated. [b] D and L are unknown but probably dense and layered phases, respectively. [c] The material obtained after 21 days of heating. [d] No solids were obtained even after 28 days of heating. [e] The material obtained after 28 days of heating.

the Si/Al and OH^-/Si ratios of which are exactly the same as the ratios (16 and 0.8, respectively) of the synthesis mixture of example 1 in the UOP patent,[2b] in the presence of TEA^+ only as an organic SDA. Since we were not able to observe any detectable solid from this synthesis even after 28 days of heating at 100 °C, it is clear that the addition of a supplementary organic species is required for inducing crystallization. The powder XRD patterns of the representative UZM-12 zeolites synthesized in this study are shown in Figure 1. Comparison with the XRD patterns in the literature reveals that each material is highly crystalline and no reflections other than those from the ERI structure are observed.[4] As previously reported,[2] in addition, all the X-ray peaks from the UZM-12 zeolite synthesized with Me_6-diquat-4 are much broader than those from the zeolites prepared with any of the other diquaternary ammonium ions, suggesting its nanocrystalline nature.

The overall synthesis results in Table 1 reveal that the formation of UZM-12 is strongly affected by both the central polymethylene chain length of the diquaternary cation employed as an organic crystallization SDA and its end group size. For example, we were able to synthesize this high-silica analogue of erionite using Me_6-diquat-4 or Me_6-diquat-6 in combination with TEA^+ and K^+ ions, which is consistent with the results reported by UOP researchers.[2] When the organic crystallization SDA is changed from Me_6-diquat-6 to Me_6-diquat-7, a slightly longer diquaternary cation, in addition, there was an increase in crystallization time from 14 to 21 days at 100 °C. In

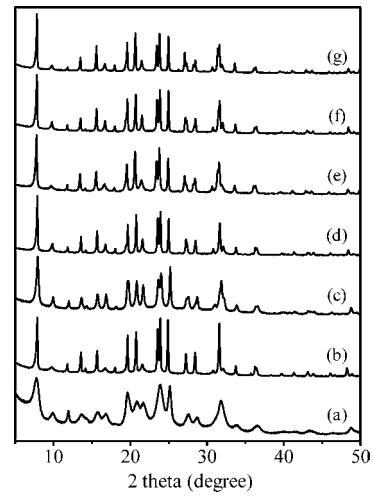

Figure 1. Powder XRD patterns of the as-made form of UZM-12 zeolites prepared using (a) Me_6-diquat-4, (b) Me_6-diquat-6, (c) Me_4Et_2-diquat-4, (d) Me_4Et_2-diquat-5, (e) Et_4Me_2-diquat-4, (f) MPr_2-diquat-4, and (g) MPp_2-diquat-4 as an organic crystallization SDA, respectively, together with TEA^+ and K^+ ions. All the zeolites were obtained after 14 days of heating at 100 °C.

particular, the use of Me_6-diquat-8 gave no detectable solids even after 28 days of heating. While the synthesis mixture containing Me_6-diquat-3, which is shortest among this series of diquaternary ammonium ions, remains amorphous after crystallization at 100 °C in a rotated autoclave for 14 days, on the other hand, its mother liquor has become dark brown. This suggests that unlike the other longer diquaternary cations in the same series, Me_6-diquat-3 may decompose easily into smaller organic fragments that cannot give UZM-12, probably due to its low thermal stability under the highly basic synthesis conditions (pH > 13) employed here. A quite similar interpretation can be made for the other five diquaternary ammonium ions with the same chain length as that of Me_6-diquat-3 but larger end groups, because neither of them directed the synthesis of UZM-12 (Table 1).

The strong influence of the central chain length of diquaternary alkylammonium ions on the crystallization of UZM-12 was also found in syntheses using the other series of diquaternary cations with larger end groups. When the end group becomes gradually bigger from the trimethyl moiety through the dimethylethyl and diethylmethyl moieties to the triethyl one, in particular, even the tetramethylene derivative (i.e., Et_6-diquat-4) yielded no crystalline products even after 28 days of heating at 100 °C. Hence, there is an upper limit to the size of the groups on the diquaternary ammonium ions in UZM-12 synthesis, as well as to the length of its central chain, which should be closely related to the dimensions (6.3 Å in diameter and 13.0 Å in height) of *eri* cages in this small-pore zeolite.[5] We have also tested the ability of diquaternary ammonium ions containing cyclic moieties like 1-methylpyrrolidinium or 1-methylpiperidinium group as organic crystallization SDAs in UZM-12 synthesis. As seen in Table 1, both MPr_2-diquat-4 and MPp_2-diquat-4 gave this zeolite after 14 days of heating, implying that the free diameters of their cyclic moieties are not larger than the diameter (6.3 Å) of *eri* cages. However, their longer polymethylene derivatives showed a notable increase in crystallization time or yielded no crystalline solids even after 28 days of heating.

Table 1 also shows that when K^+ is replaced by the equal amount of Na^+, the synthesis mixture remains amorphous even

Table 2. Stabilization Energies Calculated for the TEA^+ and Different Diquaternary Ammonium Ions Encapsulated within the *eri* Cages of ERI-Type Zeolites

organic SDA	stabilization energy, kJ mol^{-1} of SDA	UZM-12 formation[a,b]	organic SDA	stabilization energy, kJ mol^{-1} of SDA	UZM-12 formation[a,b]
TEA^+	−108.8	−			
Me_6-diquat-3	−166.4	−	Et_6-diquat-3	−83.9	−
Me_6-diquat-4	−191.5	+	Et_6-diquat-4	−63.1	−
Me_6-diquat-5	−195.6	+	Et_6-diquat-5	−13.6	−
Me_6-diquat-6	−166.7	+	Et_6-diquat-6	57.4	−
Me_6-diquat-7	−168.8	•			
Me_6-diquat-8	−65.0	−			
Me_4Et_2-diquat-3	−173.4	−	MPr_2-diquat-3	−208.8	−
Me_4Et_2-diquat-4	−199.7	+	MPr_2-diquat-4	−193.3	+
Me_4Et_2-diquat-5	−207.6	+	MPr_2-diquat-5	−176.0	+
Me_4Et_2-diquat-6	−170.2	•	MPr_2-diquat-6	−133.8	•
Me_4Et_2-diquat-7	−115.0	−	MPr_2-diquat-7	−61.1	−
Me_4Et_2-diquat-8	−58.6	−	MPr_2-diquat-8	23.6	−
Et_4Me_2-diquat-3	−139.7	−	MPp_2-diquat-3	−198.8	−
Et_4Me_2-diquat-4	−200.5	+	MPp_2-diquat-4	−134.7	+
Et_4Me_2-diquat-5	−136.0	•	MPp_2-diquat-5	−102.0	•
Et_4Me_2-diquat-6	−89.2	−	MPp_2-diquat-6	17.7	−
Et_4Me_2-diquat-7	−4.5	−[c]			

[a] The oxide composition of synthesis mixtures used is $13TEAOH \cdot 2RBr_2 \cdot 1.5KCl \cdot 0.5Al_2O_3 \cdot 16SiO_2 \cdot 400H_2O$, where R is diquaternary alkylammonium ion. Crystallization was performed under rotation (60 rpm) at 100 °C. [b] + and • indicate that UZM-12 crystallized after 14 and ≥28 days of heating at 100 °C, respectively. − indicates that the synthesis mixture remained amorphous or as a clean solution even after 28 days of heating. [c] No synthetic experiments were performed.

after 28 days of heating at 100 °C, regardless of the type of the diquaternary ammonium ion used as an organic crystallization SDA. When employing Li^+ and Cs^+ as an inorganic crystallization SDA, in addition, we always obtained a dense or layered phase and analcime (ANA), respectively. However, the combined use of Rb^+ and any of diquaternary ammonium ions that proved to crystallize UZM-12 in the presence of K^+ and TEA^+ ions gave the same zeolite product. These results clearly show that the ability of alkali cations as a crystallization SDA in UZM-12 synthesis is more selective than that of diquaternary alkylammonium ions. Because we were able to obtain this small-pore zeolite using each of more than 10 diquaternary ammonium ions with different polymethylene chain lengths and/or end group sizes as a new organic crystallization SDA, diquaternary organic additives appear to play a generally beneficial but structurally nonspecific space-filling role in the crystallization of UZM-12. As described above, however, their addition to synthesis mixtures containing TEA^+ and K^+ or Rb^+ ions is a requisite to UZM-12 synthesis, reflecting that they may have some degree of specificity in structure-directing properties. To confirm this, we replaced Me_6-diquat-6, one of already known crystallization SDAs yielding UZM-12, in the potassium aluminosilicate synthesis mixture by its specific precursors (e.g., 1,6-DBH and TMA) and performed zeolite synthesis while keeping all other parameters constant. We were able to crystallize UZM-12 in the presence of 1,6-DBH and TMA with a molar ratio of 1:3 after 14 days of heating at 100 °C. Since the use of either 1,6-DBH or TMA as a crystallization SDA always gave no detectable solids under the optimized conditions for UZM-12 formation even after 28 days of heating, it is not difficult to expect that 1,6-DBH and TMA react themselves to form Me_6-diquat-6 in situ and then to give UZM-12, as will be evidenced below. This is also the case of 1,4-dibromobutane and 1-methylpyrrolidine: UZM-12 was also synthesized by directly introducing them with a molar ratio of 1:3, instead of their diquaternary ammonium product (i.e., MPr_2-diquat-4), in the synthesis mixture.

To gain information on the host−guest interactions in UZM-12, we have calculated stabilization energies for diquaternary alkylammonium ions employed here, as well as for TEA^+, within the *eri* cage via computer modeling studies. As listed in Table 2, a stabilization energy of −109 kJ mol^{-1} of SDA was calculated for TEA^+. Because this value is considerably higher than that of any of the diquaternary ammonium ions leading to the successful UZM-12 formation, it is most likely that TEA^+ is acting as a CDM SDA rather than as a crystallization one. The calculation results in Table 2 also show that the stabilization energies for all diquaternary ammonium ions except those for their trimethylene derivatives correlate well with the experimental observations of an increase in crystallization time. This supports the speculation given above that the diquaternary organic species connected by the shortest trimethylene chain are highly unstable than the other species with longer central chains under synthesis conditions studied here. In particular, the abrupt lowering of the stabilization energy observed at a specific chain length for a given series of diquaternary ammonium ions coincides with a failure to isolate crystalline solids even after 28 days of heating. A similar trend can also be observed for the cations with the same chain length but different end group sizes, which should be attributed to differences in the geometrical constraints and van der Waals interactions of the encapsulated organic species with the *eri* cage in UZM-12.

Figure 2 shows the energy-minimized conformations of six representative diquaternary ammonium ions within the *eri* cages, all of which proved to give UZM-12 after heating at 100 °C for 14 days under the synthesis conditions described above. When only the rotation with respect to the C−N bond involving the methyl carbons of methyl groups is considered, all the C−C bonds in the tetramethylene chain of Me_6-diquat-4 were found to adopt an all-trans configuration upon encapsulation into the *eri* cage. This is not unexpected because the dimensions (4.3 Å in diameter and 10.7 Å in length) of the free Me_6-diquat-4 molecule are rather smaller than those (6.3 Å in diameter and 13.0 Å in height) of the *eri* cage. A similar configuration can also be observed for the central chains of Me_4Et_2-diquat-4 and Me_6-diquat-6. Unlike the case of Me_4Et_2-diquat-4, however, each C−C bond in the hexamethylene chain of Me_6-diquat-6 is fairly deviated from the ideal trans configuration to fit within the *eri* cage, probably due to the free length (13.3 Å) of this diquaternary cation comparable to the cage height (13.0 Å). As seen

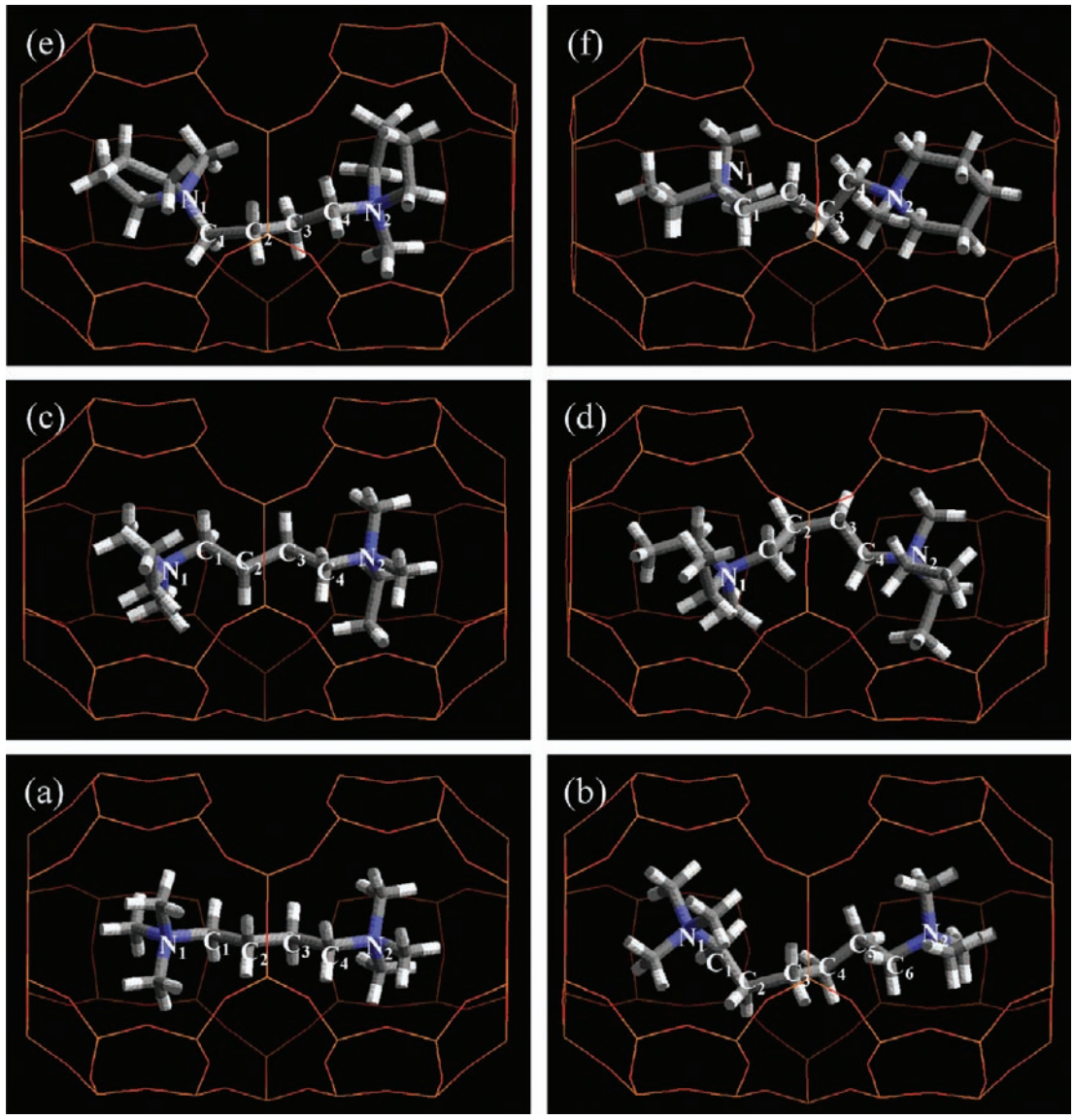

Figure 2. Energy-minimized conformations of (a) Me_6-diquat-4, (b) Me_6-diquat-6, (c) Me_4Et_2-diquat-4, (d) Et_4Me_2-diquat-4, (e) MPr_2-diquat-4, and (f) MPp_2-diquat-4 ions within *eri* cages, all of which proved to give UZM-12 after 14 days of heating at 100 °C (see Table 1). In each case C atoms are represented by gray sticks, N atoms by blue sticks, and H atoms by white sticks.

in Table 2, in fact, the stabilization energy for Me_6-diquat-6 was calculated to be higher by ca. 25 kJ mol^{-1} of SDA than that for Me_6-diquat-4. We also note that the C_2-C_3 bond in the tetramethylene chain of Et_4Me_2-diquat-4 adopts a gauche configuration, but the other two C−C bonds in the corresponding chain do a trans configuration. As seen in Figure 2, on the other hand, the two 1-methylpyrrolidinium rings in MPr_2-diquat-4 are positioned to be perpendicular to each other within the *eri* cage. By contrast, both 1-methylpiperidinium rings in MPp_2-diquat-4 are accommodated to be parallel along the long axis of *eri* cages, while being rotated by approximately 90° with each other. Therefore, it is clear that the conformation of diquaternary ammonium ions within the *eri* cage is highly influenced not only by the length of their polymethylene chains, but also by the size of the end groups on the ammonium ion, again supporting their structurally nonspecific role as a crystallization SDA in UZM-12 synthesis.

Table 3 lists the chemical compositions of nine selected UZM-12 zeolites that were synthesized using one of the diquaternary alkylammonium ions employed here, with both TEA^+ and K^+ ions present. Many of these zeolites exhibit a nonnegligible imbalance between the number of framework Al atoms (confirmed by ^{27}Al MAS NMR; see below) and sum of organic and K^+ cations compensating for framework negative charges. This suggests that a small fraction of TEA^+ and/or of ammonium groups on diquaternary organic cations occluded exists probably in the hydroxide form to serve as a space-filling species rather than as a charge-compensating cation. Table 3 also shows an enrichment of Al in all products with respect to their synthesis mixtures. In particular, there is a very high enrichment of diquaternary cations (R^{2+}), given the TEA^+/R^{2+} ratio (6.5) of synthesis mixtures, indicating their highly decisive role as an organic crystallization SDA compared to TEA^+.

Figure 3 shows the SEM images of six representative UZM-12 zeolites obtained in our study. As inferred from the powder XRD patterns in Figure 1, the UZM-12(I) material synthesized with Me_6-diquat-4 shows the smallest crystallite size (ca. 30 nm in diameter and ca. 100 nm in length) among the zeolites prepared here. Since crystallite size is inversely proportional to

Table 3. Chemical Composition Data for Selected UZM-12 Zeolites Prepared Using Different Diquaternary Ammonium Ions as Crystallization SDAs together with TEA^+ and K^+ Ions

material ID	diquaternary cation used	%N	%C	%H	%Σ[a]	C/N	unit cell composition[b]	Si/Al[c]	TEA^+/R^{2+}
UZM-12(I)	Me_6-diquat-4	2.9	12.8	3.5	19.1 (18.4)	5.2	$\|(Me_6\text{-diquat-4})_{1.8}TEA_{0.1}K_{1.2}(H_2O)_{33.0}\|\ [Al_{4.9}Si_{31.1}O_{72}]$	6.3 (3.1)	0.06
UZM-12(II)	Me_6-diquat-5	2.5	12.3	3.4	18.2 (18.2)	5.6	$\|(Me_6\text{-diquat-5})_{1.6}TEA_{0.1}K_{1.6}H_{0.4}(H_2O)_{14.0}\|\ [Al_{5.3}Si_{30.7}O_{72}]$	5.8 (3.4)	0.06
UZM-12(III)	Me_6-diquat-6	2.5	13.1	3.3	18.8 (19.6)	6.1	$\|(Me_6\text{-diquat-6})_{1.6}TEA_{0.1}K_{2.1}H_{0.9}(H_2O)_{10.3}\|\ [Al_{6.3}Si_{29.7}O_{72}]$	4.7 (3.5)	0.06
UZM-12(IV)	Me_4Et_2-diquat-4	2.3	12.7	3.3	18.4 (22.4)	7.1	$\|(Me_4Et_2\text{-diquat-4})_{1.5}TEA_{0.3}K_{2.4}OH_{0.9}(H_2O)_{15.0}\|\ [Al_{4.8}Si_{31.2}O_{72}]$	6.5 (3.7)	0.20
UZM-12(V)	Me_4Et_2-diquat-5	2.2	12.8	3.2	18.2 (21.3)	7.5	$\|(Me_4Et_2\text{-diquat-5})_{1.4}TEA_{0.2}K_{2.3}OH_{0.5}(H_2O)_{7.5}\|\ [Al_{4.8}Si_{31.2}O_{72}]$	6.5 (3.8)	0.14
UZM-12(VI)	Et_4Me_2-diquat-4	2.1	13.1	3.2	18.3 (19.2)	6.3	$\|(Et_4Me_2\text{-diquat-4})_{1.2}TEA_{0.5}K_{2.4}H_{0.3}(H_2O)_{6.9}\|\ [Al_{5.6}Si_{30.4}O_{72}]$	5.5 (3.6)	0.42
UZM-12(VII)	MPr_2-diquat-4	2.3	13.7	2.8	18.7 (19.4)	6.7	$\|(MPr_2\text{-diquat-4})_{1.8}TEA_{0.2}K_{2.3}OH_{1.0}(H_2O)_{10.8}\|\ [Al_{5.1}Si_{30.9}O_{72}]$	6.0 (3.6)	0.11
UZM-12(VIII)	MPr_2-diquat-5	2.1	14.3	3.2	19.6 (18.8)	7.3[d]	$\|(MPr_2\text{-diquat-5})_{1.6}TEA_{0.2}K_{2.2}H_{0.1}(H_2O)_{7.8}\|\ [Al_{5.5}Si_{30.5}O_{72}]$	5.5 (3.7)	0.13
UZM-12(IX)	MPp_2-diquat-4	2.3	15.2	3.5	20.9 (22.3)	7.9[d]	$\|(MPp_2\text{-diquat-4})_{1.4}TEA_{0.7}K_{2.3}OH_{0.3}(H_2O)_{9.1}\|\ [Al_{5.5}Si_{30.5}O_{72}]$	5.6 (3.4)	0.50

[a] The total organic content in wt%. The values in parentheses are exothermic weight losses by TGA/DTA at 250−800 °C. [b] Determined by a combination of elemental and thermal analyses. The water content was calculated from the endothermic weight loss by TGA/DTA up to 250 °C, and H^+ or OH^- has been introduced to make the as-made zeolites electrically neutral. [c] The values in parentheses are the Si/Al ratios calculated from the ^{29}Si MAS NMR data. [d] The numbers of diquaternary alkylammonium and TEA^+ ions per unit cell of these materials were determined from the curve deconvolution of their ^{13}C MAS NMR spectra, because the C/N ratios (7.5 and 8.0) of MPr_2-diquat-5 and MPp_2-diquat-4 are very close to or the same as the ratio (8.0) of TEA^+, making it almost impossible reasonably determine the numbers of the occluded diquaternary alkylammonium and TEA^+ ions by elemental analysis.

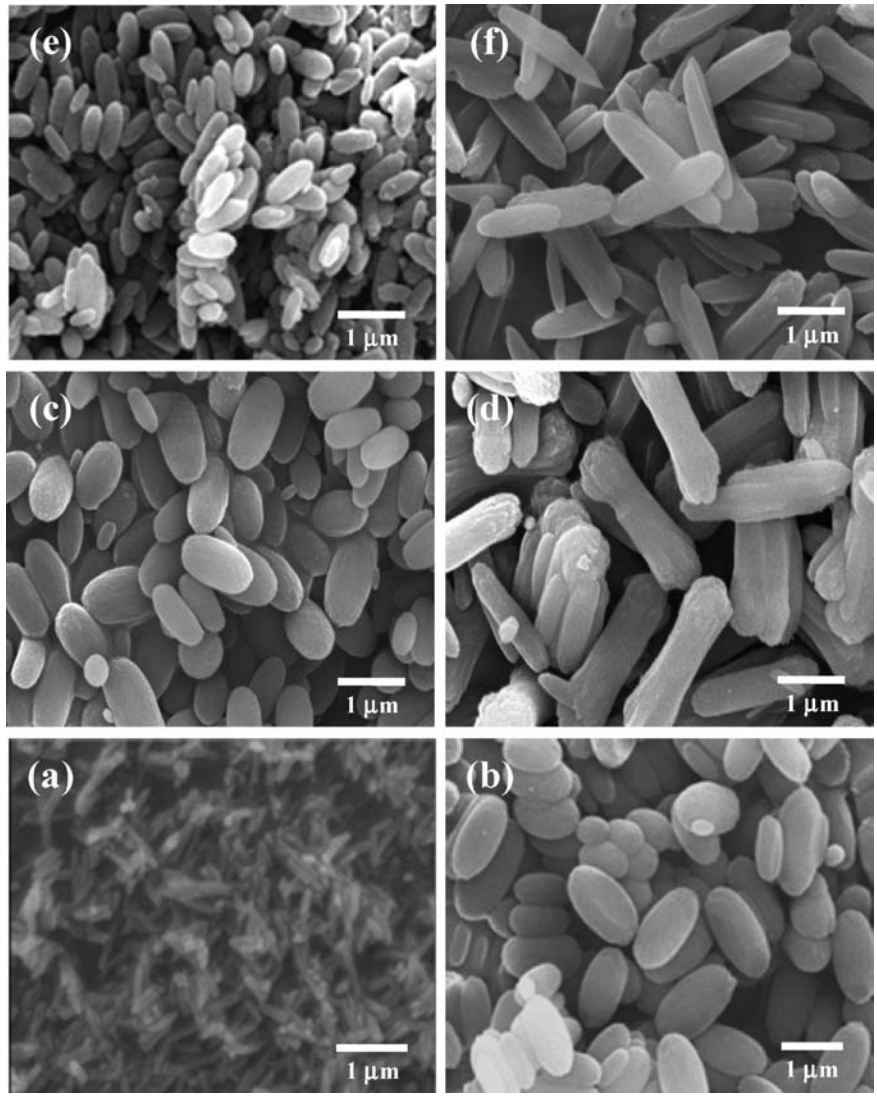

Figure 3. SEM images of UZM-12 zeolites prepared in the presence of (a) Me_6-diquat-4, (b) Me_6-diquat-6, (c) Me_4Et_2-diquat-5, (d) Et_4Me_2-diquat-4, (e) MPr_2-diquat-4, and (f) MPp_2-diquat-4 as an organic crystallization SDA, respectively, in combination with TEA^+ and K^+ ions.

the number of nuclei, the ability of Me_6-diquat-4 to form UZM-12 nuclei appears to be better than that of any of diquaternary organic cations employed in this study. Another interesting observation is a trend of increasing the crystallite size of UZM-12 with increasing the central polymethylene chain length of diquaternary ammonium ions or their end group size. For example, the UZM-12(II) material obtained in the presence of Me_6-diquat-5, a slightly longer organic cation than Me_6-diquat-

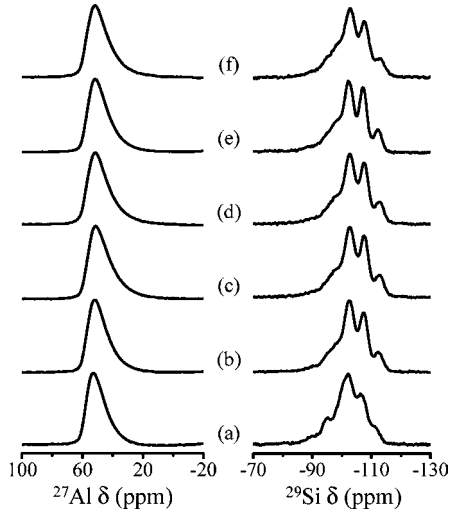

Figure 4. ^{27}Al (left) and ^{29}Si (right) MAS NMR spectra of as-made (a) UZM-12(I), (b) UZM-12(III), (c) UZM-12(V), (d) UZM-12(VI), (e) UZM-12(VII), and (f) UZM-12(IX) that were synthesized using Me_6-diquat-4, Me_6-diquat-6, Me_4Et_2-diquat-5, Et_4Me_2-diquat-4, MPr_2-diquat-4, and MPp_2-diquat-4 as an organic crystallization SDA, respectively, in combination with TEA^+ and K^+ ions.

4, consists of rice grains of 150 nm ×400 nm (Supporting Information Figure S1). When again changing the organic crystallization SDA from Me_6-diquat-5 to Me_6-diquat-6, the UZM-12 zeolite crystallized has a quite similar morphology but a considerably larger crystallite size of 600 nm ×1000 nm. Such an increase in crystallite size can also be found in comparison of the SEM images of the three UZM-12 materials prepared using Me_6-diquat-4, Me_4Et_2-diquat-4, and Et_4Me_2-diquat-4, as an organic crystallization SDA, respectively (Figure 2 and Supporting Information Figure S1). By contrast, the use of Rb^+ instead of K^+ as an inorganic crystallization SDA gave no significant changes in the UZM-12 crystallite morphology and size.

A combination of the ^{1}H−^{13}C CP MAS and ^{13}C MAS NMR spectra of the six UZM-12 zeolites described above clearly shows that each diquaternary alkylammonium ion used as an organic crystallization SDA remains intact upon its occlusion into the UZM-12 cavities (Supporting Information Figure S2). The fact that the ^{13}C resonances from TEA^+ are hardly observable for all UZM-12 zeolites is consistent with the chemical composition data in Table 3. Comparison with the liquid ^{13}C NMR spectra of the dibromide salt of the corresponding diquaternary ammonium ions reveals that the degree of geometric constraints and van der Waals interactions of the occluded organic species with the zeolite framework may vary not only with the central chain length of the diquaternary cation employed, but also with its end group size, as evidenced by molecular simulation results in Figure 2. The ^{1}H−^{13}C CP MAS NMR spectrum of UZM-12 obtained using a mixture of 1,6-DBH and TMA with a molar ratio of 1:3, instead of Me_6-diquat-6, after heating at 100 °C for 14 days can be found in Supporting Information Figure S3. Since the presence of Me_6-diquat-6 in this UZM-12 material is confirmed, the in situ formation of many other diquaternary ammonium ions during the synthesis, once they yield UZM-12, is also likely to occur.[9c]

Figure 4 shows the ^{27}Al and ^{29}Si MAS NMR spectra of six selected UZM-12 zeolites in the as-made form. While the ^{27}Al MAS NMR spectra of these materials exhibit only one broad line around 53 ppm, typical of tetrahedral Al sites, the spectra

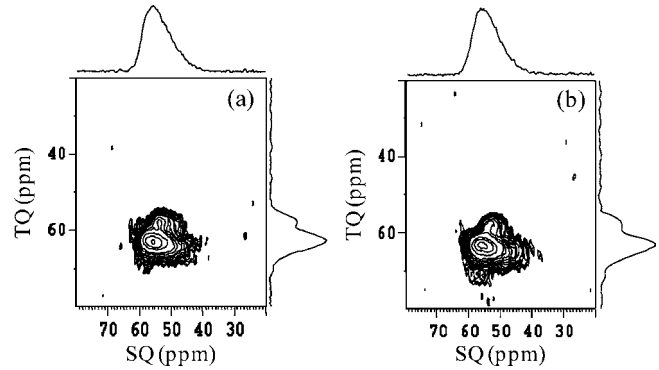

Figure 5. ^{27}Al 3Q MAS NMR spectra of as-made (a) UZM-12(I) and UZM-12(III). Their ^{27}Al 3Q MAS isotropic projection spectra are given at the right of the 2D 3Q MAS NMR plot.

of their proton form give an additional resonance around 0 ppm (Supporting Information Figure S4). This indicates that a portion of framework Al atoms has been extracted from the UZM-12 framework during the calcinations and ion exchange steps. Since all H-UZM-12 zeolites including H-UZM-12(I) have comparable octahedral Al fractions to one another, however, it appears that the nanocrystallinity itself may not have a harmful effect on the thermal stability of zeolites, as previously reported.[14,27] As seen in Figure 4, on the other hand, the ^{29}Si MAS NMR spectra of the six UZM-12 zeolites are characterized by four ^{29}Si lines around −97, −102, −107, and −112 ppm with no significant differences in the relative intensity ratio. A similar line shape was also observed for the other as-made UZM-12 zeolites prepared in this work. Attempts to deconvolute these spectra by assuming each of the four Si(*n*Al) lines with $n = 3$, 2, 1, and 0 as a single Si environment and a random Al distribution over the two crystallographically distinct tetrahedral sites (T-sites) with multiplicities of 24:12 of the UZM-12 framework gave $(Si/Al)_{NMR}$ ratios of 3.1−3.8 that are considerably lower than the ratios (4.7−6.5) determined by elemental analysis (Table 3). This suggests that not only the T-O-T angle range for the two crystallographically distinct T-sites is not narrow enough to get into a single ^{29}Si line envelope, but also the Al distribution over the two T-sites is nonrandom.

To obtain clear evidence for the speculation given above, we have performed ^{27}Al 3Q MAS NMR measurements on the as-made UZM-12(I) and UZM-12(III) materials synthesized using Me_6-diquat-4 and Me_6-diquat-6 as an organic crystallization SDA, respectively. As seen in Figure 5, the ^{27}Al 3Q MAS isotropic projection spectra of both zeolites reveal two contributions around 63 and 55 ppm in the framework tetrahedral Al region. When using the equation of Jacobsen et al.,[28] the average Al−O−Si angles for the high- and low-field ^{27}Al resonances were calculated to be 139.5 and 150.5°, respectively. These values are in good agreement with the average T_1-O-T and T_2-O-T angles (142.0 and 151.1°, respectively) derived from Rietveld refinements of the powder synchrotron diffraction data for a natural zeolite erionite with Si/Al = 2.75,[29] despite the notable difference in Si/Al ratios for the two ERI-type zeolites compared. The relative intensity ratios of the two ^{27}Al reso-

(27) Camblor, M. A.; Corma, A.; Valencia, S. *Microporous Mesoporous Mater.* **1998**, *25*, 59.
(28) Jacobsen, H. S.; Norby, P.; Bildsøe, H.; Jakobsen, H. J. *Zeolites* **1989**, *9*, 491.
(29) Gualtieri, A.; Artioli, G.; Passaglia, E.; Bigi, S.; Viani, A.; Hanson, J. C. *Am. Mineral.* **1998**, *83*, 590.

Table 4. NMR Parameters and Relative Intensities Determined from the ^{27}Al MAS/3Q MAS NMR Spectra of As-Made UZM-12(I) and UZM-12(III) Zeolites

			Al_1(4Si)			Al_2(4Si)			
material	diquaternary cation used	Si/Al[a]	δ_{iso},[b] ppm	P_Q,[c] MHz	I, %	δ_{iso},[b] ppm	P_Q,[c] MHz	I, %	$I(Al_1)/I(Al_2)$
UZM-12(I)	Me_6-diquat-4	6.3	62.6	2.4	79	54.9	1.7	21	3.8
UZM-12(III)	Me_6-diquat-6	4.7	63.2	2.5	83	55.5	1.5	17	4.9

[a] Determined by elemental analysis. [b] Isotropic chemical shifts and second-order quadrupolar parameters, respectively, estimated from the ^{27}Al 3Q MAS NMR data in Figure 5. The error range for each δ_{iso} is $\pm$0.3 ppm and that for $P_Q \pm 0.2$ MHz. [c] Isotropic chemical shifts and second-order quadrupolar parameters, respectively, estimated from the ^{27}Al 3Q MAS NMR data in Figure 5. The error range for each δ_{iso} is $\pm$0.3 ppm and that for $P_Q \pm 0.2$ MHz.

Table 5. Characterization Data for MTO Catalysts Employed in This Study

catalyst	diquaternary cation used	Si/Al ratio[a]	crystallite shape and average size,[b] nm	BET surface area,[c] $m^2\ g^{-1}$	micropore volume,[d] $cm^3\ g^{-1}$	mesopore volume,[e] $cm^3\ g^{-1}$	no. of surface *eri* cages/g solid,[f] $\times 10^{18}$	amount of coke deposited,[g] wt %
H-UZM-12(I)	Me_6-diquat-4	6.3	needles, 30 × 100	512	0.09	0.74	96.5 (22.1)	9.2
H-UZM-12(II)	Me_6-diquat-5	5.8	rice grains, 100 × 400	623	0.22	0.28	28.3 (6.5)	14.4
H-UZM-12(V)	Me_4Et_2-diquat-5	6.5	rice grains, 600 × 1100	675	0.28	0.13	5.3 (1.2)	16.5
H-UZM-12(VI)	Et_4Me_2-diquat-4	5.5	rods, 650 × 2500	627	0.25	0.10	4.4 (1.0)	20.4
H-UZM-12(VII)	MPr_2-diquat-4	6.0	rice grains, 350 × 800	642	0.26	0.16	8.8 (2.0)	23.3
H-SAPO-17	–	0.04	needles, 500 × 3000	610	0.21	0.10	–	13.5
H-SAPO-34(I)	–	0.21	cuboids, 1000	754	0.27	0.03	–	20.1
H-SAPO-34(II)	–	0.21	cuboids, 2000−4000	804	0.28	0.08	–	22.3
H-SSZ-13	–	5.1	heavily overlapped cuboids, 2000−5000	856	0.29	0.12	–	22.4

[a] Determined by elemental analysis. [b] Determined by SEM. [c] Calculated from N_2 adsorption data. [d] In the diameter range $\leq$15 Å. [e] In the 20- to 500-Å diameter range. Calculated using the BJH formalism. [f] Calculated by assuming that each H-UZM-12 zeolite is composed of ideal cylinders. The values given in parentheses are the relative ratios referenced to the number of the surface *eri* cages of H-UZM-12(VI) with the largest crystallite size among the UZM-12 zeolites prepared here. [g] The amount formed during MTO at 350 °C and 0.67 h^{-1} WHSV for 10 h on stream. Determined by TGA/DTA up to 800 °C.

nances determined from the ^{27}Al MAS/3Q MAS NMR spectra of as-made UZM-12(I) and UZM-12(III) are given in Table 4. Both zeolites gave considerably larger relative intensity ratios (3.8:1 and 4.9:1, respectively) than the ideal value (2:1) expected for the statistical distribution of Al atoms over the two sites T_1 and T_2 with Loewenstein's rule. This indicates a preferential Al substitution into the high-multiplicity site (i.e., site T_1) during the crystallization of UZM-12, unlike the result previously reported for erionite zeolites with Si/Al = 2.8−4.0.[30]

Table 5 lists the physical properties of all small-pore materials examined for the MTO reaction, and Figure 6 compares their NH_3 TPD profiles. Although the crystallite sizes of the five H-UZM-12 zeolites are notably different from one another, there are no significant differences in the total area of NH_3 desorption (i.e., the density of acid sites) as expected from the similarity in Al contents. This is also the case of the temperature maxima (250−300 and 400−450 °C, respectively) of their two desorption peaks. Because the number and strength of acid sites among these ERI-type catalysts are not so large, comparison of their MTO performance will allow us to illustrate the crystallite size effects.[17a,31] As seen in Figure 6, on the other hand, the strong acid sites in H-SAPO-17 possess a slightly lower strength and a narrower strength distribution than those in its aluminosilicate analogues. However, the strength of strong acid sites is considerably higher in H-SSZ-13 than in H-SAPO-34(I) or H-SAPO-34(II), as previously ascertained by IR spectroscopy with adsorbed CO.[32] These results are consistent with the general

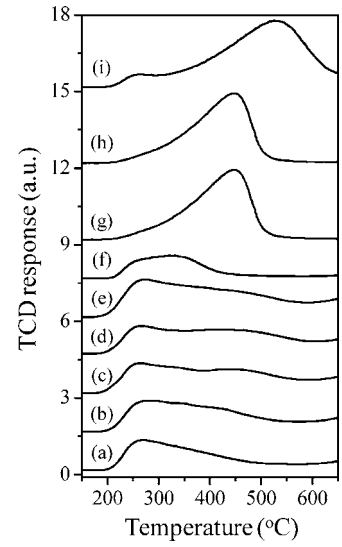

Figure 6. NH_3 TPD profiles from (a) H-UZM-12(I), (b) H-UZM-12(II), (c) H-UZM-12(V), (d) H-UZM-12(VI), (e) H-UZM-12(VII), (f) H-SAPO-17, (g) H-SAPO-34(I), (h) H-SAPO-34(II), and (i) H-SSZ-13.

consensus that the acidic properties of zeolitic materials can differ according to both their framework topology and composition.[33]

Figure 7 shows the MeOH conversion as a function of TOS in the MTO reaction over the proton form of a series of H-UZM-12 catalysts with similar Al contents (Si/Al = 6.0 ± 0.5) but different crystallite sizes at 350 °C and 0.67 h^{-1} WHSV. It can be seen that the H-UZM-12(I) material with the smallest crystallite dimensions among the UZM-12 zeolites synthesized here exhibits an initial MeOH conversion of almost 0%. When DME is considered as a product, however, it shows an initial

(30) (a) Lillerud, K. P.; Raeder, J. H. *Zeolites* **1986**, *6*, 474. (b) Lillerud, K. P. *Zeolites* **1987**, *7*, 14.
(31) (a) Wilson, S.; Barger, P. *Microporous Mesoporous Mater.* **1999**, *29*, 117. (b) Chen, D.; Moljord, K.; Fuglerud, T.; Holmen, A. *Microporous Mesoporous Mater.* **1999**, *29*, 191.
(32) Bordiga, S.; Regli, L.; Cocina, D.; Lamberti, C.; Bjørgen, M.; Lillerud, K.-P. *J. Phys. Chem. B* **2005**, *109*, 2779.
(33) Lercher, J. A.; Jentys, A. *Stud. Surf. Sci. Catal.* **2007**, *168*, 435.

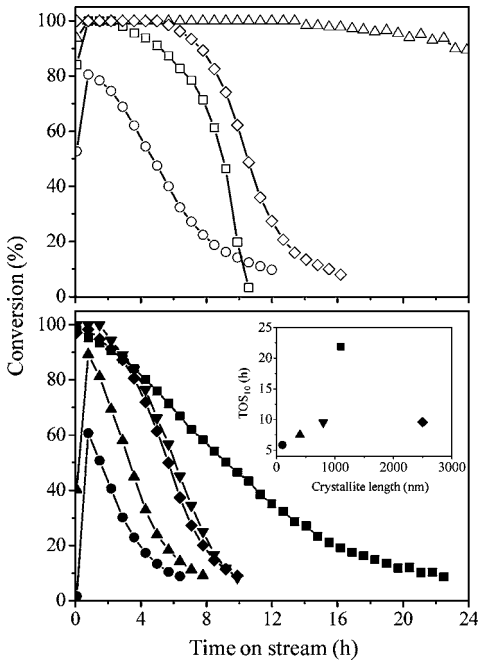

Figure 7. MeOH conversion as a function of TOS in MTO over H-UZM-12(I) (●), H-UZM-12(II) (▲), H-UZM-12(V) (■), H-UZM-12(VI) (♦), H-UZM-12(VII) (▼), H-SAPO-17 (○), H-SAPO-34(I) (Δ), H-SAPO-34(II) (□), and H-SSZ-13 (◇) at 350 °C and 0.67 h^{-1} WHSV. The inset shows a plot of time on stream (TOS_{10}) for decreasing the methanol conversion over each H-UZM-12 zeolite to 10% versus its crystallite length.

conversion of ca. 85% (Supporting Information Figure S5), indicating that the DME molecules formed within this nanocrystalline zeolite easily escape its *eri* cages before being converted to olefins. A similar result, although less pronounced, can also be observed for the H-UZM-12(II) catalyst with the second smallest crystallite size. Therefore, the very low initial MeOH conversion observed for these two H-UZM-12 zeolites cannot be associated with the kinetic induction period of the MTO process observed for cage-based, small-pore materials.[16] As seen in Figure 7, by contrast, the other three H-UZM-12 materials with larger crystallite sizes show MeOH conversions of 100% or so from the beginning of the reaction.

Like H-SAPO-34, UZM-12 is also a cage-based, small-pore material. Therefore, it is not very difficult to reason that after some TOS olefin formation over this ERI-type zeolite should be dominated by the so-called hydrocarbon pool mechanism,[16] in which organic reaction centers act as scaffolds for producing mainly ethene ($C_2^=$) and propene ($C_3^=$) within its *eri* cages. If such were the case, crystallite size would then play a crucial role in determining the deactivation rate of UZM-12 zeolites as previously reported.[31] However, the actual situation is more complex, since there is no inverse correlation between their crystallite size and period of TOS for decreasing the MeOH conversion to 10% (Figure 7). While the H-UZM-12(V) material consisting of rice grains of ca. 600 nm ×1100 nm exhibits the highest stability among the H-UZM-12 zeolites studied here, the most rapid deactivation was observed for H-UZM-12(I) with the smallest crystallite size. The characterization results in Table 5 reveal that the micropore volume (0.09 $cm^3\ g^{-1}$) of H-UZM-12(I) is much smaller than the volume of any of the other four H-UZM-12 zeolites, but it has a much larger mesopore volume (0.74 $cm^3\ g^{-1}$). Assuming an ideal cylindrical morphology for these five UZM-12 zeolites with different crystallite sizes, in fact, the number of the *eri* cages (i.e., surface cages) located on the external surface of H-UZM-12(I) crystallites was calculated to be approximately 20 times larger than that of the analogous cages on the external surface of the equivalent weight of H-UZM-12(V) crystallites (Table 5). The same is also true for the numbers of the acid sites within outer *eri* cages of these two H-UZM-12 zeolites, since their Si/Al ratios are almost identical with each other. Therefore, it should be much more difficult for the former nanocrystalline zeolite than for the latter microcrystalline one to keep olefin molecules formed over within the *eri* cage and thus to convert them to active organic reaction centers, for example, to hexamethylbenzene on H-SAPO-34.[34] This taken in total lead us to believe that the nanocrystallinity of zeolitic materials has a harmful effect on their MTO activity and stability, especially when they are for cage-based topologies.

Figure 7 also compares the MTO performance of H-SAPO-17, H-SAPO-34(I), SAPO-34(II), and H-SSZ-13. Unlike H-SAPO-34(I), which is still active even after 24 h on stream, H-SAPO-34(II) with a larger crystallite size (2000−4000 nm) is almost deactivated within 10 h on stream. As a result, H-SAPO-34(II) exhibits lower MTO stability than H-UZM-12(V). However, it is clear from Figure 7 that CHA-type materials having no *can* cages have better MTO stability than ERI-type ones, despite the much higher density and strength of strong acids in the former materials (Figure 6). This suggests that the framework topology of cage-based, small-pore molecular sieves is a more critical factor affecting MTO stability than their acidity or crystallite size.[35] On the other hand, H-SAPO-17 has fairly higher and lower stability than H-UZM-12(I) and H-UZM-12(V), respectively. However, no noticeable differences are found in comparison with the other three H-UZM-12 materials, probably due to the similarity in acidity of these ERI-type materials. The yields of light olefins and the $C_2^=/C_3^=$ ratio as a function of TOS in MTO over H-UZM-12(I), H-UZM-12(V), H-SAPO-17, H-SAPO-34(I), and H-SSZ-13 measured under reaction conditions described above are shown in Figure 8. These data reveal that after some TOS, ERI-type materials show higher $C_2^=/C_3^=$ ratios than CHA-type ones, probably due to the considerably lower density and strength of strong acids in the former materials (Figure 6).

Figure 9 shows the GC−MS total ion chromatograms of CCl_4 extracts obtained by dissolving H-UZM-12(I), H-UZM-12(V), and H-SAPO-17 in HF after MTO at 350 °C and 0.67 h^{-1} WHSV as a function of TOS, together with the assignments of the observed peaks made by comparing their mass spectra with those in the NIST database.[26] The detectable aromatic hydrocarbon species formed on the nanocrystalline H-UZM-12(I) material after 0.75 h on stream, when the catalyst is most active during the period of TOS studied, include polymethylbenzenes with 4−6 methyl groups and polymethylnaphthalenes with 3−5 methyl groups. Also, polymethylated anthracenes and phenanthrenes are detectable in H-UZM-12(I) when almost deactivated after 6 h on stream, which tempted us to consider them as the main species responsible for the catalyst deactivation. However, this is not the case, because such tricyclic aromatic compounds were already found in the microcrystalline H-UZM-12(V) only after 0.75 h on stream when not deactivated at all (Figure 7). Therefore, the rate of their formation is much faster on H-UZM-12(V) than on H-UZM-12(I), probably due to the less severe

(34) Arstad, B.; Kolbe, S. *J. Am. Chem. Soc.* **2001**, *123*, 8137.
(35) (a) Park, J. W.; Lee, J. Y.; Kim, K. S.; Hong, S. B.; Seo, G. *Appl. Catal., A* **2008**, *339*, 36. (b) Castro, M.; Warrender, S. J.; Wright, P. A.; Apperley, D.; Belmabkhout, Y.; Pirnberger, G.; Min, H.-K.; Park, M. B.; Hong, S. B. *J. Phys. Chem. C* **2009**, *113*, 15731.

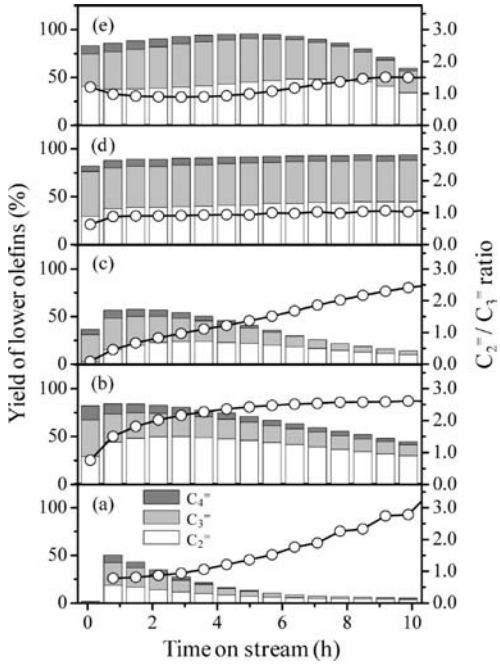

Figure 8. Yields in lower olefins and $C_2^=/C_3^=$ ratio as a function of TOS in MTO over (a) H-UZM-12(I), (b) H-UZM-12(V), (c) H-SAPO-17, (d) H-SAPO-34(I), and (e) H-SSZ-13 at 350 °C and 0.67 h^{-1} WHSV.

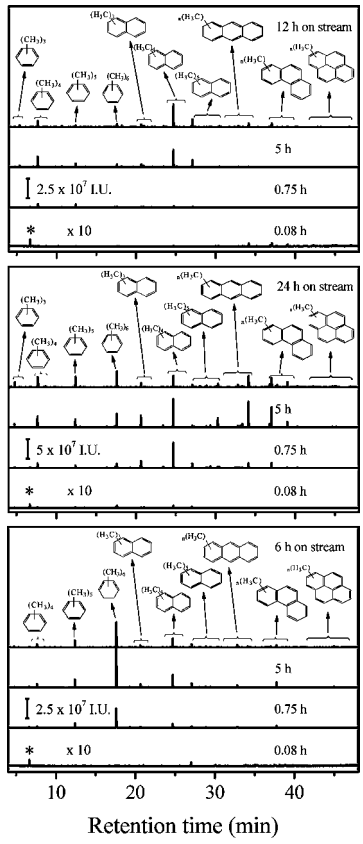

Figure 9. GC−MS total ion chromatograms of CCl_4 extracts from H-UZM-12(I) (bottom), H-UZM-12(V) (middle), and H-SAPO-17 (top) catalysts obtained by dissolving in HF after MTO at 350 °C and 0.67 h^{-1} WHSV for different periods of TOS. The structures annotated onto the chromatograms are peak identifications having compared the mass spectra to those in the NIST database.[26] The asterisk represents the mass signal of C_2Cl_6 produced by pyrolysis of CCl_4.

diffusion of MeOH in the latter material, leading to a lower concentration of intrazeolitic reactant and product molecules that should retard the formation of polycyclic aromatic hydrocarbons. In fact, the amount (9.2 wt %) of coke formed on H-UZM-12(I) during 10 h on stream was found to be considerably smaller than that observed for any of the other eight zeolitic materials studied here (Table 5). This led us to conclude that the intracrystalline buildup of large organic compounds (i.e., coke) in H-UZM-12(I) cannot be the main origin of the fast deactivation of this nanocrystalline zeolite.

It is interesting to note here that while the formation of phenanthrene in deactivated H-SAPO-34(II) and H-SSZ-13 with the CHA topology is clearly detectable, this is not the case of methylphenanthrenes (Supporting Information Figure S6). As seen in Figure 9, however, the opposite trend was observed for deactivated H-UZM-12 and H-SAPO-17 with the ERI topology. We also found that methylanthracenes, which are slightly narrower but longer than methylphenanthrenes, were always detected in all ERI-type materials, whereas their formation in H-SAPO-34(II) is negligible even when fully deactivated. Because the dimensions ($6.3 \times 6.3 \times 13.0$ Å^3) of *eri* cages in latter topology are slightly narrower but longer than those ($6.7 \times 6.7 \times 10.0$ Å^3) of *cha* cages in the former topology, it is clear that the cage shape in cage-based, small-pore materials, as well as their size, may be a critical factor governing the type of the accumulated aromatic hydrocarbon species during MTO and, hence, the activity and deactivation behavior.[20,35,36] This suggests that during MTO the empty inorganic cages themselves may be acting as reverse templates for the formation of a particular class of polyaromatic hydrocarbons whose size and shape are closely related to the cage dimensions.

On the other hand, it has long been suggested that methane (C_1) formation over H-ZSM-5 (MFI) during MTO may occur via direct methylation of the coke deposits on this medium-pore zeolite with MeOH followed by C_1 elimination, unlike the case of other higher alkanes.[37] Very recently, we have shown that H-ZSM-5 with a relatively high Al content (Si/Al = 14), which begins to be rapidly deactivated after ~20 h on stream at 400 °C and 4 h^{-1} WHSV, exhibits a sudden increase in C_1 selectivity at a similar TOS,[20] due to the pore blockage instead of intrazeolitic active site coverage by coke deposition on the external surface of zeolite crystallites during MTO.[38] Since C_1 selectivity can be regarded as a useful measure of examining catalyst deactivation in this reaction, we have therefore compared the C_1 selectivities of H-UZM-12(I) and H-UZM-12(II) with the two smallest crystallite sizes and poorest MTO activities among the zeolitic materials studied here, with those of H-UZM-12(V) and H-SAPO-34(I). As seen in Figure 10, H-UZM-12(I) with a number of *eri* cages on the outer crystallite surface about 20 times larger than that of H-UZM-12(V) (Table 5) and, hence, a much larger number of external acid sites exhibits a continuous increase in C_1 selectivity up to 80% during ca. 12 h on stream, when it is almost deactivated. A similar trend can also be observed for the other nanocrystalline zeolite H-UZM-12(II) except for a notable decrease in C_1 selectivity at the beginning of the reaction. However, the microcrystalline H-UZM-12(V)

(36) Bleken, F.; Bjørgen, M.; Palumbo, L.; Bordiga, S.; Svelle, S.; Lillerud, K.-P.; Olsbye, U. *Top. Catal.* **2009**, *52*, 218.
(37) Schulz, H.; Böhringer, W.; Baumgärtner, W.; Zhao, S. *Stud. Surf. Sci. Catal.* **1986**, *28*, 915.
(38) (a) Karge, H. G.; Boldingh, E. P. *Catal. Today* **1988**, *3*, 53. (b) Bjørgen, M.; Svelle, S.; Joensen, F.; Nerlov, J.; Kolboe, S.; Bonino, F.; Palumbo, L.; Bordiga, S.; Olsbye, U. *J. Catal.* **2007**, *249*, 195.

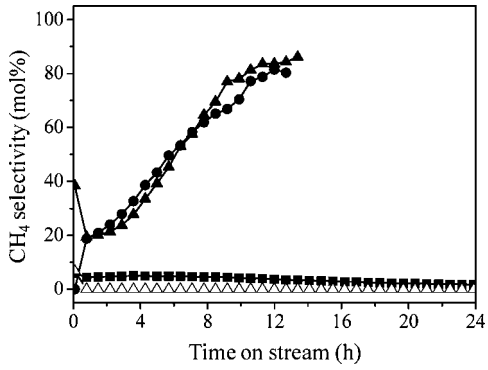

Figure 10. Selectivity to methane as a function of TOS in MTO over H-UZM-12(I) (●), H-UZM-12(II) (▲), H-UZM-12(V) (■), and H-SAPO-34(I) (Δ). The reaction conditions are the same as those given in Figure 7.

material with a much smaller number of external acid sites is characterized by much lower and constant C_1 selectivities (∼5%) during the period of TOS studied, similarly to H-SAPO-34(I). Therefore, we conclude that the poor stability observed for nanocrystalline H-UZM-12 materials may be mainly due to the fast formation of polycyclic coke molecules on the external surface of their nanocrystallites, rendering intrazeolitic acid sites inaccessible for MTO. From a catalytic point of view, this is instructive in that 'nano' is not always better than 'micro'.

Conclusions

The synthesis of zeolite UZM-12 using a number of flexible, linear diquaternary alkylammonium ions as organic crystallization structure-directing agent (SDA), in combination with tetraethylammonium and alkali metal cations, has been investigated. More than ten diquaternary ammonium ions with different polymethylene chain lengths and alkylammonium group sizes were found to be new organic crystallization SDAs for the synthesis of this ERI-type zeolite. Computer modeling studies suggest that all of them match well within the large cylindrical *eri* cages of the ERI topology, and ^{27}Al MQ MAS NMR experiments evidence a preferential Al substitution into the high-multiplicity site in UZM-12 zeolites during their synthesis. The overall catalytic results of our study demonstrate that decreasing the crystallite size of cage-based, small-pore materials from the micrometric to the nanometric range (probably the ≤100-nm range) has a harmful effect on their MTO activity and stability because of the intensive coke buildup on the external surface of their crystallites that may limit the diffusion of methanol molecules to intrazeolitic acid sites and thus make them inaccessible for catalysis in the long run.

Acknowledgment. This work was supported by the National Research Foundation of Korea (R0A-2007-000-20050-0 and 2009-0092793) and by the Carbon Dioxide Reduction and Sequestration R&D Center (16-2008-02-005-01). We thank Prof. J. A. van Bokhoven (ETH Zurich) for ^{27}Al 3Q MAS NMR measurements. We also thank one reviewer for the valuable comments.

Supporting Information Available: Complete ref 1a and additional information as noted in the text. This material is available free of charge via the Internet at http://pubs.acs.org.

JA105185R